SAND2006-1588C

ILASS Americas, 19th Annual Conference on Liquid Atomization and Spray Systems, Toronto, Canada, May 2006

Effects of Air on Splashing During a Droplet Impact

Richard A. Jepsen[§], Sam S. Yoon[*], Byron Demosthenous[‡]
[§]Mechanical Environments, [‡]Applied Diagnostics, Sandia National Lab, P.O. Box 5800, Albuquerque, NM 87185-1135. * Mechanical Engineering Department, Korea University, Anamdong, 5-Ga, Sungbukgu, Seoul, 136-713, Korea.

Abstract

Recent studies have shown the importance of air in causing the splashing phenomenon and subsequent finger formation for a liquid droplet impact. While previous work focused on the experimental aspect and addressed the issues associated with the Rayleigh-Taylor instability, additional experimental investigation and the relevant computational modeling have been performed to gain additional insight on the large scale splashing phenomenon. Previously reported modeling efforts have not considered the effect of air by starting the simulation at the time of droplet-liquid contact with the substrate. Here, we start the simulation using the VOF (volume of fluid) method at a location one diameter upstream so that the compressed air effect due to a falling droplet is properly taken into account. Both the experiments and simulations demonstrate that the displaced air obtains momentum from a falling droplet and induces a vortex motion immediately above the contact surface as it is ejected. The splashing (or ejection) occurs when the initial edge of the impacting and spreading liquid is entrained into the displaced and accelerated air. It is also hypothesized that the perturbation generated during the splashing process is radially propagated and is the fundamental instability that eventually forms fingers at the rim of the spreading liquid.

[§]Corresponding author: rajepse@sandia.gov

Introduction

Droplet impact phenomena are readily encountered in raindrop impact and in numerous industrial applications such as inkjet printing, painting, spray-wall impact within the IC-engine, and fire suppression sprays. We are particularly interested in large liquid slug impact and dispersion phenomenon as shown in **Fig. 1** [12] where a tank filled with dyed water (2830 kg) impacts an unyielding wall at the speed of 100 m/s or greater; the Weber number for this case is on the order of ~10^8 which far exceeds the previously reported studies limited to $We = \rho D U_{imp}^2 / \sigma < 5 \times 10^4$ [2-11,13-42] (where ρ, U_{imp}, D, and σ are the liquid density, impact speed, droplet diameter, and the liquid surface tension). These large scale tests are difficult to repeat and instrument with the diagnostics necessary to measure details of the fluid structure during break-up and dispersion. Therefore, several smaller scale tests are being performed to investigate the impact and break-up phenomena for large water droplets or slugs (~0.1 m diameter) at large Weber number (1×10^4 to 1×10^6).

As per well-known classical experiments [13], a droplet is known to stick to the impacting surface at a relatively high impact Weber number when the droplet surface tension energy is not high enough to overcome the droplet's dissipative energy [27]. Upon sticking, the droplet spreads radially and forms a toroidal ring at a relatively low Weber number. At an intermediate Weber number, an azimuthal instability develops and forms "fingers" at the rim of the spreading ring. If the Weber number is increased even more, the droplet "splashes" at the first contact with the surface prior to the finger formation. This transitional behavior, splashing, plays a significant and dominant role in the droplet impact at extremely high impact speed as in **Fig. 1**; only splashing occurs without any spreading.

Figure 1. Dispersed water (dyed red) at furthest extent radially from impact [12]. Frame is approximately 92 m wide and is 2 seconds after impact.

The classical Rayleigh-Taylor (R-T) instability [3, 43-48], in which heavy fluid accelerates toward a light fluid, is known to appear as fingers at the fluid-fluid interface. Allen [3] suggested that the observed fingers at the front of the ring of liquid spreading after droplet impact were caused by an R-T instability due to the radial expansion of the liquid into the surrounding air. While Allen's idea has been accepted among the researchers [25-26,41], Thoroddsen and Sakakibara [22] claimed that the fundamental instability of the fingering phenomenon is due to the initial undulation which imprints on the radially expanding jet at the very first stage of the contact between a falling liquid droplet and the solid substrate.

Recently, Xu et al. [1] reported the importance of air in causing the splashing, which also seemed to affect the fingering instability as in **Fig. 2**; when there is no splashing due to the reduced atmospheric pressure, there is no finger formation, and vice versa. Xu et al. [1] stated that splashing occurs because of compressed air while the initially contacted liquid rim flows outward but is pushed back by air resistance, deflecting its motion and resulting in added momentum in the vertical direction. This initial perturbation may be responsible for the finger formation later. The recent experiment by Yoon et al. [2] supported that Thoroddsen and Sakakibara [22] and Xu et al. [1]'s claim on the importance of the initial perturbation due to air by showing that the ejecting splashed liquid is always accelerated by the compressed escaping air, which results in the splashed droplet speed always being greater than the droplet impact speed. For further details, see Ref. [2].

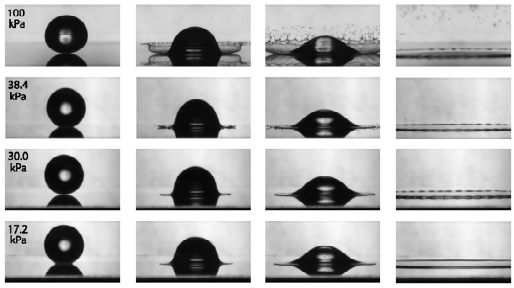

Figure 2. Recent experiment by Xu et al. [1] of the University of Chicago. Neither the splashing nor finger formation occurred when the atmospheric pressure decreased. Reprinted with the permission of Prof. Sidney R. Nagel of University of Chicago.

In this paper, we present additional experimental data (with respect to Ref. [2]) and examine the compressed air effect on the splashing and the subsequent fingering phenomenon using the VOF (volume of fluid) method. The VOF approach was previously used [5-7,10] for modeling the liquid droplet impact. However, it is important to note that

all the previous modeling efforts [4-11] began their simulation at the time on which the impacting droplet was in contact with the substrate and, thus, the air effect due to the collapsing droplet cannot be well resolved. Here, we start our simulation at one diameter upstream location from the impacting surface, which has enabled us to computationally investigate the effect of the escaping/accelerated air on splashing.

Modeling

Computational Details

To investigate the dynamics of compressed air, a liquid sphere impacting on a solid surface is simulated using a 2D, two-phase flow Navier-Stokes (NS) solver (Stormflow, *Adaptive Research*), which utilizes the conventional VOF (Volume of Fluid) method [49]. Even though the current computational effort is limited to 2D (and, thus, not directly applicable for the actual comparisons with the experimental results), it is useful using the current computational tool to obtain qualitative predictions on the behavior of the compressed air due to a falling droplet.

The NS solver, based on a Reynolds-averaged Navier Stokes (RANS) formulation employing a standard k-ε isotropic turbulence closure model of Nallasamy [50], is coupled with the Lagrangian droplet tracking model [51-52]. The gas-phase flow is calculated on a Eulerian staggered Cartesian grid using the pressure correction method of the SIMPLEC algorithm [53]. The second order upwinding and centered scheme are used for the convective and diffusion terms, respectively, in solving the transport differential equations. The droplet phase evolves using a Lagrangian approach based on the stochastic separated flow model [51-52]. The momentum equation for a small rigid sphere in a non-uniform flow of Maxey and Riley [54] is used and the drag model of Faeth [51] is used.

The computational domain for our simulation extends 0.4 m x 0.1 m using a 95×50 grid resolution that is symmetric about the droplet centerline. The computational node is carefully chosen after the verification of the solution independence from the grid resolution. The diameter of the impacting droplet is 0.1 m and the impact speed is 10 m/s. The grid resolution in the droplet impact area (0.1m X 0.1m) was refined to 50 X 50 cells. The time step for the calculation was 2×10^{-5} s. Most of the parametric runs requires the computational time of less than 1 day. A 'stair-step' grid is applied to resolve the smooth circular shape of the droplet in a Cartesian coordinate system. This stair-step grid is unavoidable in VOF method as mentioned by Pasandideh-Fard et al [10] and Bussmann et al [25] unless the method is timely modified by or coupled with the finite element method [8] or boundary integral method [11,23]. Since the computational results are based on the 2D mode, the direct comparison against the experiment is not applicable but does provide much insight on the effects of the compressed and ejected air.

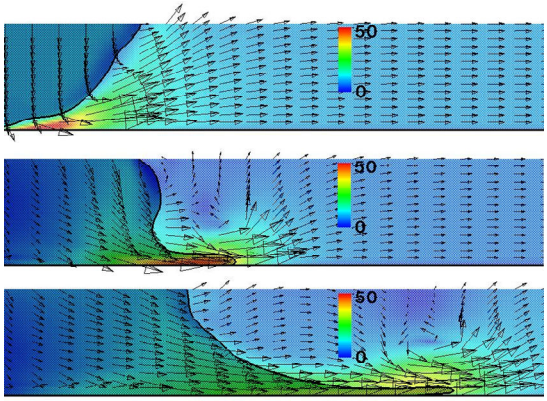

Figure 3. Evolution of the induced air due to a falling droplet at t = 0, 2, and 4 ms. The maximum speed of the induced air nears 5 times the impact speed (i.e., U_{imp} = 10 m/s, D = 0.1 m). The color contour is scaled with the local total velocity. The light and dark regions represent the air and liquid, respectively. Note that the domain shown extends 15 cm x 3 cm. The VOF, $(\rho_{cell} - \rho_{gas})/\rho_{liq}$, value used in this contour plot is 0.5.

Entrainment of Water from Accelerated Air

In **Fig. 3**, the time series of an impacting droplet are shown. Prior to the impact, the air is compressed and accelerated up to 5 times the impact speed (U_{imp} = 10 m/s) at t = 0. It is clear that the air obtained an upward vertical momentum while being compressed due to a downwardly falling droplet. At t = 2 ms, an induced vortex rollup motion of air is observed due to spreading liquid. This rollup continues to follow the edge of the spreading liquid at t = 4 ms. At this point, the air reduces its speed as it dissipates. However, the fluid still affects the air motion (especially the air layer in contact with the moving fluid) while spreading radially.

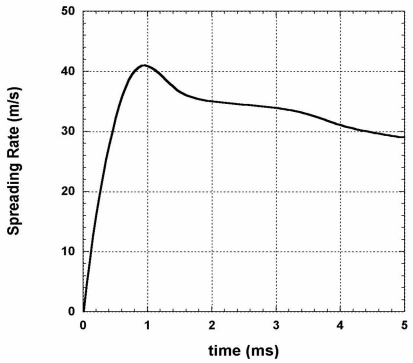

Figure 4. The spreading rate of impacting droplet shown in Fig. 3 using a VOF of 0.5 for the interface at the leading edge.

In **Fig. 4**, the liquid spreading speed (horizontal) of the case shown in **Fig. 3** is recorded. It is shown that

the liquid quickly obtains momentum within 1 ms and, thus, the fluid edge is accelerated; the air existence is the only cause which can induce such phenomenon. For 1 ms < t < 5 ms, the fluid edge decelerates because boundary layer effect starts to dominate and impede the motion of the liquid spreading.

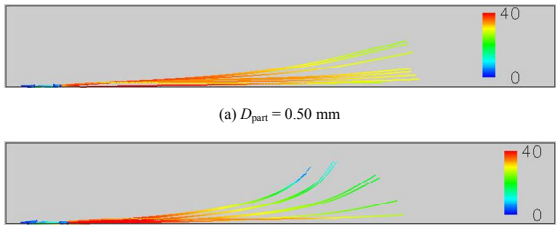

(a) D_{part} = 0.50 mm

(b) D_{part} = 0.25 mm

Figure 5. The pathlines of the ejected particles from initial ejection up to t = 8 ms for various particle sizes, (a) D_{part} = 0.50 mm and (b) D_{part} = 0.25 mm, in conjunction with Fig. 3 and Table 1. Ten particles were ejected. The color contour is scaled with the Lagrangian total droplet velocity. Note that the particle size of D_{part} = 1.0 mm (which is not shown in this figure) did not gain any vertical momentum due to its heavy weight. The domain shown extends 40 cm x 6 cm. The lower left corner is the center of the impacting droplet as in Fig. 3. Note that the atmospheric pressure is 100 kPa. The impact speed is 10 m/s.

To estimate the intensity of the fluid entrainment by the displaced and compressed air, we have located 10 liquid particles of a constant size directly under the droplet center with an initial velocity of zero. It is expected that the smaller droplets will be readily entrained by the escaping, accelerated air whereas the motion of the larger droplets will not be as intense as that of the smaller droplets. The motions of D_{part} = 0.50 mm and 0.25 mm particle shown in **Fig. 5** indicates that the results are consistent with the expected behavior; the smaller particles (D_{part} = 0.25 mm as in are lifted higher than the larger particles. **Table 1** shows the maximum lifted height (Δy_{max}) and the maximum speed (U_{max}) of the particles ranging from 0.25 mm < D_{part} < 2.00 mm. The particles, initially at rest, are accelerated (see the change in contour level from 'blue' to 'red' in **Fig. 5**) by the ejected air and then their speed is reduced due to air drag. This difference in the dynamical behavior due to particle size confirms that the accelerated air is capable of entraining and lifting small droplets, but the large particles will not be as significantly affected. In addition, the vortex roll-up at the leading edge of the interface may also contribute to the splash crown formation.

Table 1. Statistics of the traveling particle of various sizes. The droplet size and impact speed are 0.1 m and 10 m/s, respectively.

Particle Size (mm)	Δy_{max} (mm)	U_{max} (m/s)
0.25	47	45
0.50	34	42
1.00	5	26
2.00	<1	19

The ability of the escaping air to entrain and lift a liquid particle is also affected by ambient pressure. A lower air pressure (or density) is not as capable of transferring momentum to the spreading liquid or splashing particles. It should be noted that the escaping air has the same velocity in all cases since it is driven by the relative change in pressure between the compressed region near the impact and the surrounding ambient pressure. **Table 2** summarizes the model results for the same particle size at progressively lower pressures (and densities). Model results show the particles experience greatly reduced lift and entrainment as the pressure decreases. This trend is also consistent with the experimental findings of Xu et al. [1].

Table 2. Statistics of the traveling particle at various atmospheric pressures. The ejecting particle size is 0.25 mm. The droplet size and impact speed are 0.1 m and 10 m/s, respectively.

Atm. Pressure (kPa)	Δy_{max} (mm)	U_{max} (m/s)
100	47	45
70	21	39
50	9	22
30	2	19

Experiment

Experimental Apparatus

Large water slug impact experiments were done using latex bladders to transport the slugs to a clear acrylic target. Immediately prior to impact, the latex was removed using a small (0.5 cm) blade. The latex peels away from the water in less than 1 ms resulting in a large spherical water droplet shaped like the latex bladder. The disturbance to the droplet surface due to the latex quickly peeling away does not affect the compression and ejection of the air. It also does not seem to affect the finger formation since our data on finger formation is comparable to previous work for similar We (the reasons are well explained in Ref. [2]). In some tests where interactions with gas or air were measured, the latex was not removed in order to obtain a sharp leading edge of the collapsing droplet.

Data was gathered using three digital Phantom cameras (*Vision Research*, Wayne, NJ) arranged as shown in **Fig. 6(a)** with frame rates between 4,800 and 10,000 fps and exposure times from 5 to 100 µs per frame. Both forward and backlighting techniques were used. A thin CO_2 cloud layer in **Fig. 6(b)** and Schlieren method in **Fig. 6(c)** were used to observe the induced motion of the air or gas upon the droplet impact. *TrackEye* software was used to post-process the time history of the velocity of the ejecting fluid particles upon splashing. Droplet size was fixed at D = 0.1 m and the drop height varied from 1.27 m to 1.94 m, which gives the impact speed of U_{imp} = 5 m/s and 6.18 m/s.

(a)

(b)

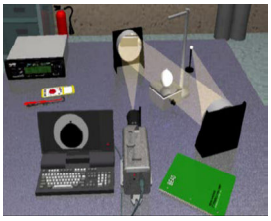

(c)

Figure 6. (a) Capturing the side view. (b) Gas cloud generation using the dry-ice. (c) Schlerian Set-up.

Experimental Results

Using the *TrackEye* software, the radial velocities of randomly chosen droplets ('splash 1', 'splash 2', and 'splash 3') are recorded as in **Fig. 7(a)**. The start time for the tracking in **Fig. 7(a)** was 7 to 27 ms after impact because the particles or spreading edge were not easily discernable at early times due to the interference and high density of splashing particles. However, all three splashed droplets show some minor acceleration ('Λ' shape) at the initial stage and then experience an air drag and, thus, their velocities reduce. The pattern of the spreading edge or ring velocity appears to be quite interesting as its value fluctuates during its spreading for the period of 28 ms < t < 45 ms. The fluctuation may be due to the pressure pulsing generated during the continuous supply of the impacting fluid. In **Fig. 7(b)**, the liquid spreading velocity from the modeling prediction (which is in conjunction with the experiment shown in Fig. 9(a)) is shown. This modeling prediction also indicates the rapid acceleration within 2 ms and the appearance of the fluctuation starting from approximately t = 23 ms up to t = 34 ms; any further recording was not possible due to the computational domain limit used for this modeling run. It is interesting to observe that the maximum radial velocity is about ~ 4 times of the impact velocity (i.e., U_{imp} = 5 m/s and $U_{rad,\ max}$ ~ 20 m/s). This trend is consistent with the case shown in **Figs 3** and **4**; U_{imp} = 10 m/s and $U_{rad,\ max}$ ~ 40 m/s. It is noteworthy that the maximum spreading radial velocity is always smaller than the maximum velocity of the accelerated/escaping air: $U_{air,\ max}$ ~ 50 m/s from **Fig 3**. Further discussions on the pressure pulsing issue are available in Ref. [2].

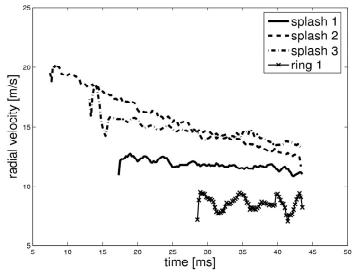

(a)

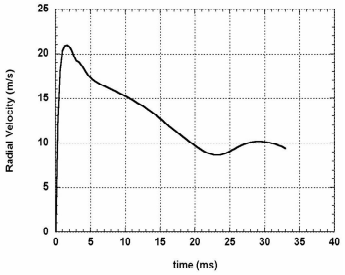

(b)

Figure 7. The spreading ring velocity ('ring 1' in the legend box): (a) from the experiment. (b) modeling prediction on the 'ring' radial velocity (using VOF model).

Figures 8 and 9 demonstrate the evolution of the induced motion of the compressed air during the collapsing phase of a falling droplet on a thin layer of CO_2 on the target surface. The photos were taken from beneath the transparent plexiglass (**Fig. 8**) and from the side (**Fig. 9**) for the same event. In this case, the latex on the balloon was not removed so the water splashing would not interfere with the air-gas interactions. Certainly, the balloon rebounds subsequent to the impact due to its excessively high surface tension force of the latex. The maximum spreading of the latex bound droplet occurs at 26 ms for this case.

Three very important observations should be noted from these tests. One is that the CO_2 gas is displaced ahead of the leading edge of the deformed impacting droplet, second is that a crown shape (3D instability) appears due to the vortex roll-up of the escaping air as the similar crown shape was formed (**Fig. 9**) by the splashing liquid droplet in **Fig. 2** (see 100 kPa case), and finally that there appears to be an "sunflower" shape 3D instability induced from the escaping air.

Tests were also done using the Schelrian technique to visualize the compressed air that is ejected upon impact and collapse of the droplet. **Fig. 10** clearly shows a jet of air ejected as the droplet begins collapsing on the surface.

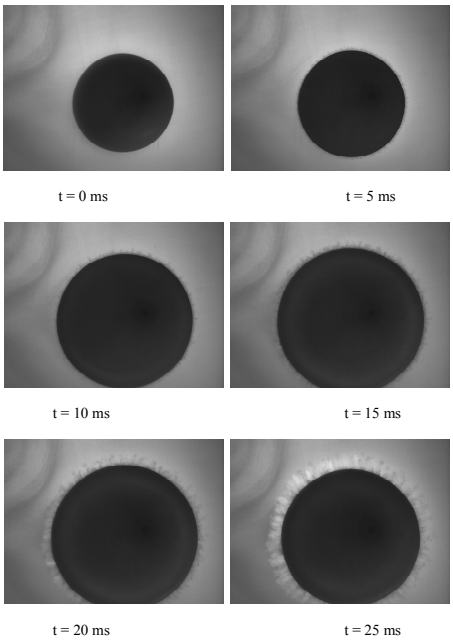

Figure 8. Evolution of the finger formation due to the induced azimuthal instability of air when a balloon hits the plexiglass surface. Photos are taken beneath the plexiglass at the bottom location.

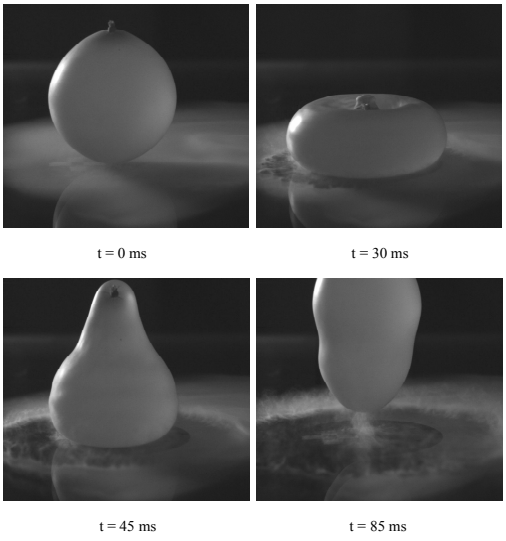

Figure 9. Side view of the experiment corresponding to Fig. 8. The balloon droplet rebounds due to its high surface tension energy.

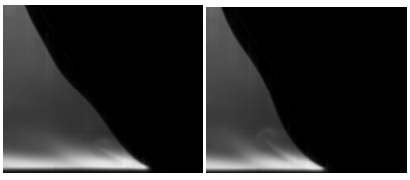

Figure 10. Development of the vortex rollup motion while air being compressed and ejected due to a falling drop.

It is worthy to re-iterate the objective of our current study. It is claimed, in this report, that the surrounding air has a profound effect on splashing speed and shape. As mentioned previously, the splashing acts as an initial perturbation for the eventual finger formation during the liquid spreading on the impact surface while the conventional thought contrarily suggests that the spreading itself causes the finger formation due to the Rayleigh-Taylor instability. To prove our claim, we focus our attention to the initial perturbation which we believe the fundamental cause of splashing. It is natural to believe that there must be some interaction between the falling droplet and the accelerated air. Certainly, the air below the falling droplet is compressed and, thus, the air density changes slightly (but the change does not exceed orders of magnitude). The shearing effect between the falling droplet and the rapidly escaping air might be significant enough to cause some disturbance at the bottom of the falling droplet and becomes the source of the initial undulation that Thoroddsen and Sakakibara [22] observed in their experiment. To show our point, we examine the wavenumbers of the maximum growth rate from both the Rayleigh-Taylor instability and the Kelvin-Helmholtz instability [55].

The dispersion relation from the Rayleigh-Taylor instability is known as below [3]:

$$\omega^2 = \frac{\rho_l - \rho_g}{\rho_l + \rho_g} gk - \frac{k}{\rho_l + \rho_g} k^3 \qquad (1)$$

where g is the acceleration/deceleration of the liquid spreading edge upon impact. The subscripts $(\,)_g$ and $(\,)_l$ represent the properties of gas and liquid, respectively. The maximum wavenumber, $k_{\max}$, corresponding to the maximum growth rate, $\omega_{\max}$, can be found by taking the derivative of the Eq. (1) with respect to the wavenumber, k and setting the derivative equal to zero.

$$k_{\max} = \sqrt{\frac{g(\rho_l - \rho_g)}{3\sigma}} \qquad (2)$$

While the dispersion relation of the Kelvin-Helmholtz instability is written as follows,

$$\omega^2 = \frac{\rho_g}{\rho_l} U_{rel}^2 k^2 - \frac{\sigma}{\rho_l} k^3 \qquad (3)$$

where U_{rel} is the relative velocity between the liquid and air. The maximum wavenumber of the Kelvin-Helmholtz instability can be obtained in the

same manner which applied to the Rayleigh-Taylor instability above.

$$k_{\max} = \frac{2}{3}\frac{U^2 \rho_g}{\sigma} \qquad (4)$$

These maximum wavenumbers in Eqs. (2) and (4) are plotted as a function of the gas density, ρ_g, as in **Fig. 11**. The gas density varies from 1 kg/m^3 (air density) to 1000 kg/m^3 (water density). The Xu et al [1] droplet characteristics are chosen for this comparison: the droplet diameter is 3.4 mm and the impact speed is 3.74 m/s. The deceleration of the spreading liquid is approximated by $g \approx U_{imp}^2 / D$ according to Aziz and Chandra [27]. The initial relative velocity between the falling droplet and the escaping air should be 5 times of the impact speed according to the modeling observation from **Fig. 4**. However, the ratio between the relative and the impact velocity is varied from 1 to 4 for a conservative estimate. When taking the limit of $\rho_g \to 0$ for the case of vacuum to be consistent with the experiment of Xu et al. [1], the Rayleigh-Taylor wavenumber indicates that the mode is still unstable as the maximum wavenumber is positive. However, the wavenumber of the Kelvin-Helmholtz instability indicates that the mode is stable as $k_{\max} \to 0$ in the limit of $\rho_g \to 0$, which is consistent with the Xu et al.'s [1] observation. In addition, the Rayleigh-Taylor theory cannot explain the sudden change of the stability mode observed in the experiment of Xu et al. [1] when the gas density changed from 1kg/m^3 to $\rho_g \to 0$ while the Kelvin-Helmholtz theory does explain the quickly changing characteristics of the instability mode for the sudden gas density change as ρ nears zero. Most liquid impact tests have been tested in the atmospheric condition where the gas density is 1 kg/m^3, whose region is shared by both the Rayleigh-Taylor instability and the Kelvin-Helmholtz instability as shown in **Fig. 11**. It may be coincidence that the experimental data were in agreement with the Rayleigh-Taylor instability because it shares the same region on **Fig 11** as the Kelvin-Helmholtz instability curves. It would certainly be interesting to compare the experimental data obtained in the higher gas density environment (such as "argon" or "nitrogen") with the instability theories mentioned above.

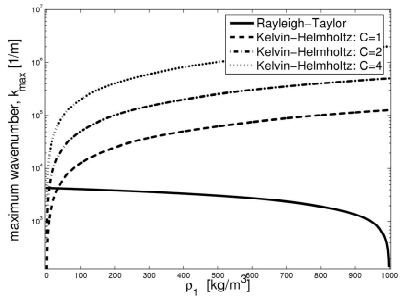

Figure 11. Maximum wavenumber comparison between the Rayleigh-Taylor and Kelvin-Helmholtz theories at various gas density, ρ_1. The Xu et al's [1] droplet is considered for this comparison: the droplet diameter is 3.4 mm, the impact speed is 3.74 m/s. For the Rayleigh-Taylor instability, the deceleration is approximated as $g \approx U_{imp}^2 / D$ according to Aziz and Chandra [27]. For the Kelvin-Helmholtz instability, the ratio between the air escaping speed and the impact speed is taken to be $C = U_{rel}/U_{imp}$ = 1, 2, and 4.

Conclusion

Both model simulation and experimental results demonstrate that the compressed and displaced air directly beneath the impacting droplet affect the splashing and spreading characteristics. Model simulations and experiments show the escaping air traveling as much as 5 times the impact velocity and creating a vortex roll-up that moves radially away from the impact region near the spreading liquid-air interface. Simulations also show the fast moving air capable of enough momentum transfer to entrain small droplets into the ejected air and even follow the vortex roll-up. However, air at reduced pressure and density has less ability to entrain the liquid. Likewise, the same phenomena are supported by experimental data. The experiments also suggest that the instability that forms fingers in the spreading liquid may be something other than the Rayleigh-Taylor instability. We suggest that the Kelvin-Helmholtz may be the fundamental source of the instability which certainly deserves the attention of the liquid impact research community for further investigation. Much of the claims in this report have not been observed in previous work because simulations started with the droplet already in contact with the surface and did not allow for compressed or displaced air. In addition, our simulations and experiments are at much higher *We* where the splashing and spreading phenomena discussed here are more pronounced.

Acknowledgement

Sandia is a multiprogram laboratory operated by Sandia Corporation, a Lockheed Martin Company, for the United States Department of Energy's National Nuclear Security Administration under contract DE-AC04-94AL85000. Our sincere thanks go to Prof. Sidney R. Nagel of University of Chicago and for providing the experimental images of **Fig 2**.

References

1. L. Xu, W. Zhang, S.R. Nagel, "Drop splashing on a dry smooth surface", *Physical Review Letter*, submitted, (2005).
2. S.S. Yoon, R.A. Jepsen, M.R. Nissen, T.J. O'Hern, "Experimental investigation on splashing and fingerlike instability of large water droplets", *Physics of Fluids*, submitted, (2006).
3. R.F. Allen, "The role of surface tension in splashing", *J. Colloid and Interface Science*, **51**, 350-351, (1975).
4. G.B. Foote, "The water rebound problem: Dynamics of collision", *The Journal of the Atmospheric Sciences*, **32**, 390-402, (1975).
5. G. Trapaga, J. Szekely, "Mathematical modeling of the isothermal impingement of liquid droplets in spraying processes", *Metallurgical Transactions B*, **22**, 901-914, (1991)
6. G. Trapaga, E.F. Matthys, J.J. Valencia, J. Szekely, "Fluid flow, heat transfer, and solidification of molten metal droplets impinging on substrates: comparison of numerical and experimental results", *Metallurgical Transactions B*, **23**, 701-718, (1992).
7. H.M. Liu, E.J. Lavernia, R.H. Rangel, "Numerical simulation of substrate impact and freezing of droplets in plasma spray processes", *Journal of Physics D*, **26**, 1900-1908, (1993).
8. J. Fukai, Z. Zhao, D. Poulikakos, C.M. Megaridis, O. Miyatake, "Modeling of the deformation of a liquid droplet impinging upon a flat surface", *Physics of Fluids A*, **5**, 2588-2599, (1993).
9. A.L. Yarin, D.A. Weiss, "Impact of drops on solid surfaces: self-similar capillary waves, and splashing as a new type of kinematic discontinuity", *J. Fluid Mech*., **283**, 141-173, (1995).
10. M. Pasandideh-Fard, Y.M. Qiao, S. Chandra, J. Mostaghimi, "Capillary effects during droplet impact on a solid surface", *Physics of Fluids*, **8**, 650-659, (1996).
11. M.R. Davidson, "Boundary integral prediction of the spreading of an inviscid drop impacting on a solid surface", *Chem. Eng. Sci*., **55**, 1159-1170, (2000).
12. R.A. Jepsen, K. Jensen, T. O'Hern, "Water dispersion modeling and diagnostics for water slug impact test", *SEM X International Congress*, (2004).
13. A.M. Worthington, *Proc. R. Soc. Lond*., **25**, 261 (1877).
14. R.F. Allen, "The mechanics of splashing", *J. Colloid and Interface Science*, **124**, 309-316, (1988).
15. S. Chandra, C.T. Avedisian, "On the collision of a droplet with a solid surface", *Proc. R. Soc. Lond*., **432**, 13-41, (1991).
16. A. Prosperetti, H.N. Oguz, "The impact of drops on liquid surfaces and the underwater noise of rain", *Annu. Rev. Fluid Mech*., **25**, 577-602, (1993).
17. M. Rein, "Phenomena of liquid drop impact on solid and liquid surfaces", *Fluid Dynamics Research*, **12**, 61-93, (1993).
18. C. Mundo, M. Sommerfeld C. Tropea, "Droplet-wall collisions: experimental studies of the deformation and breakup process", *Int. J. Multiphase Flow*, **21**, 151-174, (1995).
19. H. Marmanis, S.T. Thoroddsen, "Scaling of the fingering pattern of an impacting drop", *Physics of Fluids*, **8**, 1344-1346, (1996).
20. T. Mao, C.S. Kuhn, H. Tran, "Spread and rebound of liquid droplets upon impact on flat surfaces", *AIChE Journal*, **43**, 2169-2179, (1997).
21. G.E. Cossali, A. Coghe, M. Marengo, "The impact of a single drop on a wetted solid surface", *Exp. in Fluids*, **22**, 463-472, (1997).
22. S.T. Thoroddsen, J. Sakakibara, "Evolution of the fingering pattern of an impacting drop", *Physics of Fluids*, **10**, 1359-1374, (1998).
23. D.A. Weiss, A.L. Yarin, "Single drop impact onto liquid films: neck distortion, jetting, tiny bubble entrainment, and crown formation", *J. Fluid Mech*., **385**, 229-254, (1999).
24. M. Rieber, A. Frohn, "A numerical study on the mechanism of splashing", *Int. J. Heat and Fluid Flow*, **20**, 455-461, (1999).
25. M. Bussmann, S. Chandra, J. Mostaghimi, "Modeling the splash of a droplet impacting a solid surface", *Physics of Fluids*, **12**, 3121-3132, (2000).
26. H.Y. Kim, Z.C. Feng, J.H. Chun, "Instability of a liquid jet emerging from a droplet upon collision with a solid surface", *Physics of Fluids*, **12**, 531-541, (2000).
27. S.D. Aziz, S. Chandra, "Impact, recoil and splashing of molten metal droplets", *Int. J. Heat and Mass Transfer*, **43**, 2841-2857, (2000).
28. S.T. Thoroddsen, "The ejecta sheet generated by the impact of a drop", *J. Fluid Mech*., **451**, 373-381, (2002).

29. M.R. Davidson, "Spreading of an inviscid drop impacting on a liquid film", *Chem. Eng. Sci*., **57**, 3639-3647, (2002).
30. R. Rioboo, M. Marengo, C. Tropea, "Time evolution of liquid drop impact onto solid, dry surfaces", *Exp. in Fluids*, 33, 112-124, (2002).
31. S. Sikalo, M. Marengo, C. Tropea, E.N. Ganic, "Analysis of impact of droplets on horizontal surfaces", *Exp. Therm. and Fluid Sci*., **25**, 503-510, (2002).
32. S.L. Manzello, J.C. Yang, "An experimental study of high Weber number impact of methoxy-nonafluorobutane $C_4F_9OCH_3$ (HFE-7100) and n-heptane droplets on a heated solid surface", *Int. J. Heat and Mass Transfer*, **45**, 3961-3971, (2002).
33. I.V. Roisman, R. Rioboo, C. Tropea, "Normal impact of a liquid drop on a dry surface: model for spreading and receding", *Proc. R. Soc. Lond. A*, **458**, 1411-1430, (2002).
34. D. Sivakumar, C. Tropea, "Splashing impact of a spray onto a liquid film", *Physics of Fluids*, **14**, L85-L88, (2002).
35. A. Rozhkov, B. Prunet-Foch, M. Vignes-Adler, "Impact of water drops on small targets", *Physics of Fluids*, **14**, 3485-3501, (2002).
36. Y. Renardy, S. Popinet, L. Duchemin, M. Renardy, S. Zaleski, C. Josserand, M.A. Drumright-Clarke, D. Richard, C. Clanet, D. Quere, "Pyramidal and toroidal water drops after impact on a solid surface", *J. Fluid Mech*., **484**, 69-83, (2003).
37. C. Josserand, S. Zaleski, "Droplet splashing on a thin liquid film", *Physics of Fluids*, **15**, 1650-1657, (2003).
38. V. Mehdi-Nejad, J. Mostaghimi, S. Chandra, "Air bubble entrapment under an impacting droplet", *Physics of Fluids*, **15**, 173-183, (2003).
39. D.C.D. Roux, J.J. Cooper-White, "Dynamics of water spreading on a glass surface", *J. Colloid and Interface Sci*., **277**, 424-436, (2004).
40. S.T. Thoroddsen, T.G. Etoh, K. Takehara, Y. Takano, "Impact jetting by a solid sphere", *J. Fluid Mech*., **499**, 139-148, (2004).
41. N.Z. Mehdizadeh, S. Chandra, J. Mostaghimi, "Formation of fingers around the edges of a drop hitting a metal plate with high velocity", *J. Fluid Mech*., **510**, 353-373, (2004).
42. Y. Ge, L.S. Fan, Three-dimensional simulation of impingement of a liquid droplet on a flat surface in the Leidenfrost regime", *Physics of Fluids*, **17**, 027104, (2005).
43. D.H. Sharp, "An overview of Rayleigh-Taylor instability", *Physica*, **12D**, 3-18, (1984).
44. D.L. Youngs, "Numerical simulation of turbulent mixing by Rayleigh-Taylor instability", *Physica*, **12D**, 32-44, (1984).
45. K.I. Read, "Experimental investigation of turbulent mixing by Rayleigh-Taylor instability", *Physica*, **12D**, 45-58, (1984).
46. H. Aref, G. Tryggvason, "Vortex dynamics of passive and active interfaces", *Physica*, **12D**, 59-70, (1984).
47. T.T. Clark, "A numerical study of the statistics of a two-dimensional Rayleigh-Taylor mixing layer", *Physics of Fluids*, 15, 2413-2423, (2003).
48. S. Chandrasekha, *Hydrodynamic and Hydromagnetic Stability*, Oxford University Press, London, (1961).
49. C. W. Hirt, B.D. Nichols, "Volume of fluid (vof) method for the dynamics of free boundaries", *Journal of Computational Physics*, **39**, 201-225, (1981).
50. M. Nallasamy, "Turbulence models and their applications to the prediction of internal flows: a review", *Computers and Fluids*, **15**, 151-194, (1987).
51. G.M. Faeth, "Evaporation and combustion in sprays", *Progress in Energy and Combustion Science*, **9**, 1-76, (1983).
52. G.M. Faeth, "Mixing, transport and combustion in sprays", *Progress in Energy and Combustion Science*, **13**, 293-345, (1987).
53. S.V. Patankar, *Numerical Heat Transfer and Fluid Flow*, Taylor & Francis, New York, (1980).
54. M.R. Maxey, J.J. Riley, Equation of motion for a small rigid sphere in a non-uniform flow, *Physics of Fluids*, **26**, 883-889, (1983).
55. S.S. Yoon, S.D. Heister, Categorizing linear theories for atomizing round jets, Atomization and Sprays, **13**, 499-516, (2003).